Simulation of the CRIPT detector

Christopher Howard

Prepared by:

excelITR
102 Bank Street, 3rd Floor, Ottawa, ON Canada K1P 5N4

Contract Number: W7714-4501089282
Contract Scientific Authority: David Waller, Defence Scientist, 613-998-9985

Contract Report
DRDC-RDDC-2015-C077
March 2015

Abstract

The Cosmic Ray Inspection and Passive Tomography (CRIPT) collaboration has constructed a large-scale detector prototype for investigating the use of comic ray muon scattering tomography for Special Nuclear Material (SNM) identification. In order to fully understand the impact of various physics processes, as well as to determine the effect of systematic uncertainties (such as detector locations), a Monte Carlo simulation must be available that can reproduce the observed data. Here we present a Monte Carlo simulation that can reproduce characteristic measurements of the detectors, such as the charge deposited in each scintillator bar, as well as the number of bars hit per triggered event. The MC results can also be used to create 2D images of cargo, and achieve excellent agreement when compared to data.

This page intentionally left blank.

Table of contents

List of figures

List of tables

1 Introduction

The Cosmic Ray Inspection and Passive Tomography (CRIPT) project is an effort to construct a novel cosmic ray muon detector for the purposes of identifying Special Nuclear Material (SNM). The CRIPT collaboration has constructed a large-scale prototype at AECL's Chalk River Laboratory to investigate the merits of muon scattering tomography, wherein the three-dimensional density of a scanned object is inferred by the measured scattering of through-going charged particles. Extremely dense materials, such as SNM, can then be identified within the large three-dimensional scanning volume of the CRIPT detector.

It is important to evaluate the accuracy of the Monte Carlo (MC) simulation. The MC is capable of turing off various physics process and adding, moving, and removing material on or near the experiment. This allows analysts to identify features in the data and determine their cause. The can lead to corrections to the data, data selection criteria, and future design (or modification) considerations. The Monte Carlo can also be used in run planing and testing data analysis algorithms (*E.g.* event tracking, imaging), without the need for expensive (in time and/or money) data collection.

1.1 Detector overview

The CRIPT detector is comprised of twelve 2×2 m planes of triangular scintillator bars. Each plane contains 121 individual scintillator bars, which are 2 m long and have a triangular cross-section with a base of 3.23 cm and height of 1.65 cm. The scintillator bars are arranged in a close-fitting pattern of alternating right-side-up and up-side-down bars such that there are no gaps across the plane surface. The scintillated light from each individual bar is collected by a wavelength-shifting optical fibre which is coupled to a 64-channel photo-multiplying tube (PMT) readout device (two PMTs are needed to read out each plane).

Furthermore, the CRIPT detector is divided into six layers, where each layer contains two planes arranged orthogonally. Two layers are located above the imaging volume and are referred to as the Upper Tracker (UT), two layers are located directly below the imaging volume and are referred to as the Lower Tracker (LT), and the final two layers are located below the LT and are referred to as the Spectrometer (SPEC). Note that this report is mainly focused on the optimization of the performance of the UT and LT layers, as these layers are responsible for the tracking used for reconstructive imaging. The SPEC layers are largely ignored, as the multiple-scattering that occurs due to the steel plates (needed to perform the momentum estimate) inevitably degrades the overall SPEC performance.

2 Monte Carlo Overview

A Monte Carlo simulation (MC) is a computer program that calculates the physics processes that occur within a given geometry, provided a set of start conditions and defined primary particle characteristics. The geometry includes the shape and size of the physical components, as well as the material that each component is constructed of. To do this, we link to the GEANT4 software package[1, 2] which provides a library of physics process as well as framework to define a geometry. Initially, the current version was geant4.9.6.p02, but a major update occurred to geant4.10.00 during the course of this study. This change is detailed in Section 4, and all results have been updated to use geant4.10.00.

The data acquisition (DAQ) for the CRIPT detector[3] is processed through a custom set of procedures, through a program called anaTriangle[4]. This program outputs files for the analysts using a open-source analysis package called ROOT[5, 6], version 5.17. This is a standard analysis package in particle/nuclear physics.

The state of the CRIPT Monte Carlo was uncertain as of October 2013. Two version existed, both were partial:

1. A toy MC had some, but not all detector components, but could produce output that could be read by the data analysis tools,

2. A more complete geometry, but produced output that could not be analyzed in the same way as the data.

The problems with 1. are that we could not count on the output to be accurate, this was useful as a first-order check on some features, but no in-depth studies could be completed. 2. had more accurate results but could not be process with anaTriangle, so when differences arose between data and MC the analyst could not be confident if they due how the MC was processed or if the MC really was different than the data.

A new MC was created to replace both 1. and 2. above. The goals of this new MC were to: have accurate detector components, optimized software design, and it's output would be able to be processed through anaTriangle, in the same way as the data. This new MC would eliminate any question to the cause of features in the MC vs. data comparison. Figure 1 was produced by the new MC simulation.

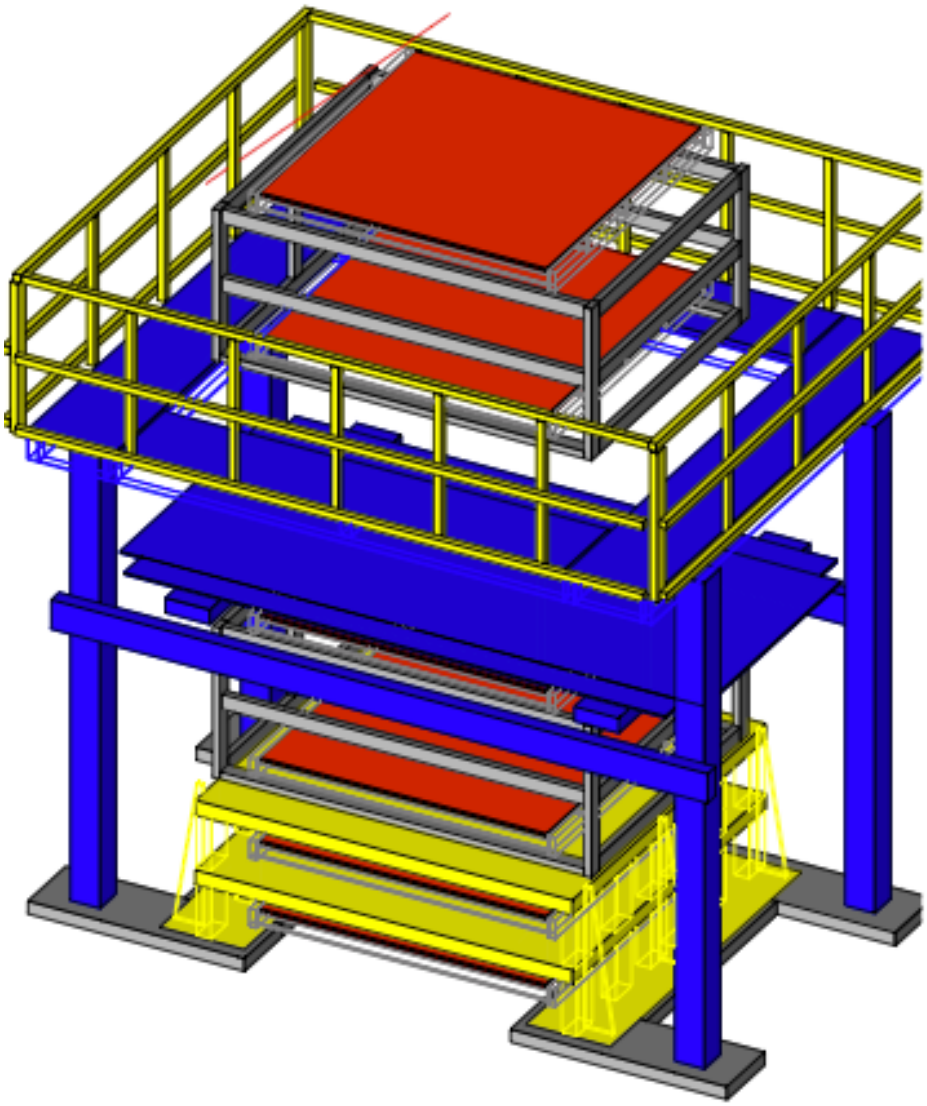

Figure 1: *The MC geometry of the CRIPT detector. The yellow bars at the top are supports for people walking the top, the blue horizontal plates are steel flooring for walking (top) and for cargo (middle). The blue horizontal beams are the support structure. The yellow plates near the bottom are the iron slabs of the spectrometer. The red plates are the panels containing the scintillator bars.*

3 Monte Carlo Geometry

The geometry of the detector is required by the GEANT4 package. The structure from the previous MCs were used as a starting point. However, it was discovered that there were simplifications used in that MC geometry that caused concern. Such as:

- Components of the geometry were overlapping,
- parts had incorrect design (solid instead of hollow),
- parts were in wrong location (eg. spectrometer iron plates).

To fix this, Computer Aided Design (CAD) drawings were provided for each component of the CRIPT detector. These dimensions and relative placement locations were used in the new MC. Figures 1 and 2 show the new detector geometry, where Figure 2 shows a cross-section of the new detector geometry. The hollow supports can now be seen to be included.

3.1 Plane Rotations

An important and necessary part of the MC is making sure the *panel* and *bar* numbering schemes matched the data. This occurs implicitly in data and MC processing, and is hard to ensure that the data and MC match. To do this two comparisons were done. 1) the charge distributions have a slope, the coordinates of the MC had to be set to match between data and MC, and 2) items were placed in the cargo during running, and the locations of these could be used to ensure the numbering scheme was implemented correctly.

This became more complicated than expected, as for historical reasons the y-coordinate in the MC was set to be vertical. The data has the vertical direction defined as the z-coordinate. This makes MC vs data comparisons difficult as there is an axis direction flip ($\hat{y}$ in MC, $\hat{z}$ in data). That is, we have (unintentionally) created a left-handed coordinate system (relative to data) in the MC. The correction is to reverse the positive-direction of the y-bars, this looks backward when drawing the geometry but is consistent with the physical detector, and so is invisible to the user, and to the definition of the geometry placement.

3.2 Plane Locations

Physical measurements were taken at Chalk River to determine where several of the lower layers and iron plates were physically located in the vertical direction. However, these measurements were taken after full assembly, so detector location within packaging was difficult to accurately determine. An algorithm to fit for the positions of the planes was developed and tested on the MC, then applied to the data. This was largely done as part

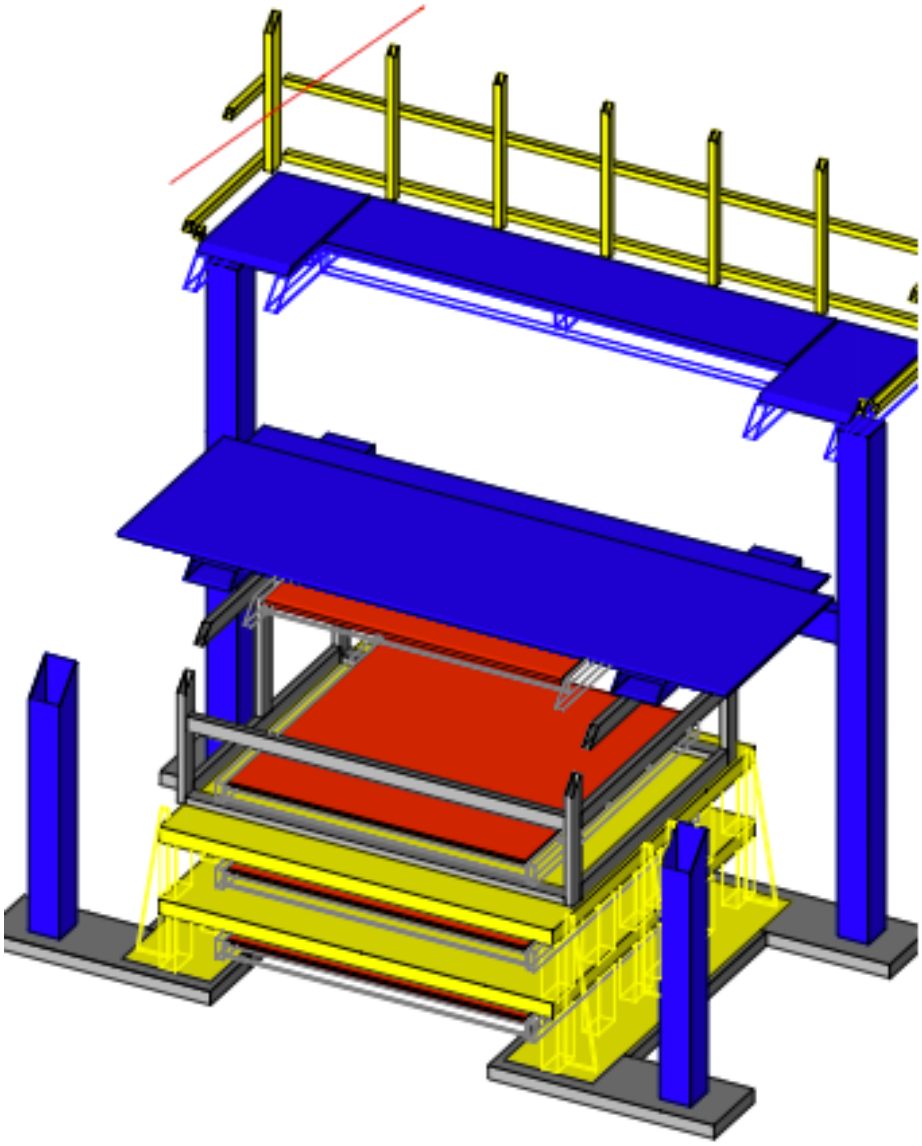

Figure 2: *Comparison of the old (left) and new (right) MC geometry.*

of Richard Hydomako's work[7]. His results were used along with measurements for the lower reference point as inputs to the MC geometry.

3.3 Bar Features

Each bar has outer measurement of height of 1.65 cm and a base of 3.23 cm. However, the entire bar was not active. The bar was constructed with an outer layer of TiO_2 which had a varying thickness. This layer was not sensitive to energy deposition from muons (or any other particles). It is included as a reflective material to aid light collection from light production in the interior active material (polystyrene scintillator).

The thickness of this had been assumed to be 0.1 mm. This assumption turned out to be an over simplification of the parameter. Figure 3 shows a photo taken of two bars. We can ignore the cloudiness of a bar, as this photo was taken for another study. Since we know the outer dimension we set a scale and measure the TiO_2 thickness along the walls. It measures to be about 0.3 mm.

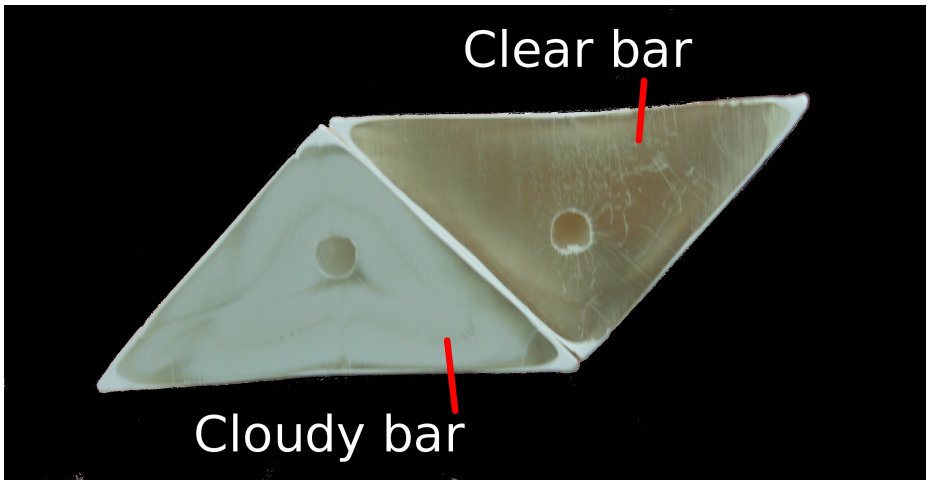

Figure 3: *Photo of two bars with the same dimensions as those used in CRIPT.*

A more important feature that can be identified from Figure 3 is the collection of TiO_2 in the *corners* of the bars. We can see that there is a much thicker layer of TiO_2 in the corners. Figure 4 is the bar geometry used in the MC, the additional TiO_2 in the corners can be seen. This additional TiO_2 has a direct impact on whether a single bar or two bars are triggered by a muon, as it increases the cross section of a single bar. The size of deposit of TiO_2 in the corners can be used as a MC tuning parameter and is discussed in Section 6.2.

3.4 Recommendation

The plane rotation is fixed, and is well known and tested. The plane locations are known by using data to fit their positions. This position fit has not been done since the reassembly

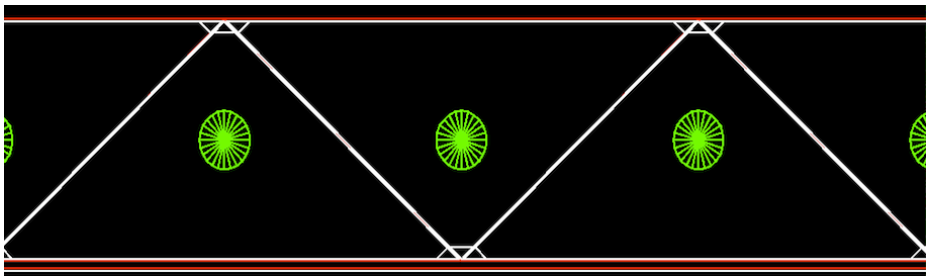

Figure 4: *CRIPT bars in the MC. The green ovals are holes in the scintillator for the fibre optic cable.*

of CRIPT at Chalk River, and will need to be updated for new data.

The additional TiO_2 in the corners and to a lesser extent the thickness of the TiO_2 along the walls will vary from bar-to-bar. In the MC, this parameter has been set to be the same for each bar, so we are averaging over all variations. Due to this implementation, this parameter can be tuned to achieve better agreement with the data.

4 Geant4 version update

At the start of this contract period (October 2013), GEANT4.9.6.p02 was the most up to date version. On December 6, 2013 the GEANT4 collaboration released GEANT4.10.00. This was a major update that changed many of the default physics within the MC. It also added multi-threading support, which is very useful modern CPUs have multiple cores that can now easily be used to increase running speed.

The MC implementation of the muon multiple scattering is the most important to an experiment like CRIPT. Tests were done to check how large of an effect the update would have on our results. To test the muon multiple scattering, we used a $20 \times 20 \times 20$ cm cube of lead. Mono-energetic (E=4 GeV) μ^-s were generated 10 cm above the centre of the block, with a direction of (0,-1,0), that is straight down in the MC. The set up and angle are shown in Figure 5. The direction of the muon exiting the block was then recorded.

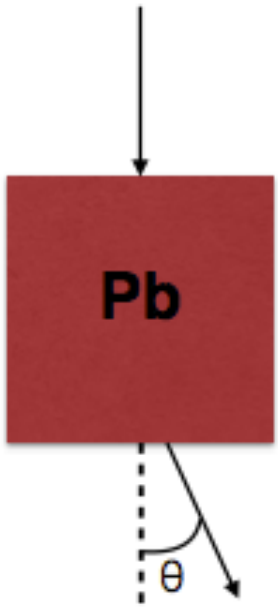

Figure 5: *A cartoon of the sep-up for Sections 4 and 5. The 4 GeV muons come from the top (0,-1,0), the red block is a* $20 \times 20 \times 20$ *cube of lead, and the scattering angle,* θ *is measured at the bottom.*

This exiting direction was then projected onto the xy-plane (where y is the vertical direction). The resulting angle is referred to as the scattering angle, θ, and is shown in Figure 6. We can see that the width in version GEANT4.9.4 differs from GEANT4.9.6 and GEANT4.10, but the latter two agree. In any case, the difference is smaller than our detector angular resolution, so this is not an issue for our analysis.

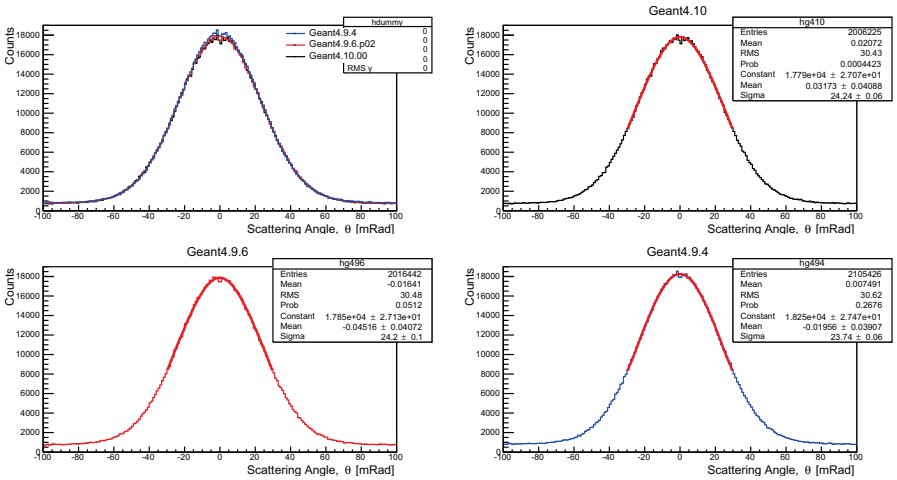

Figure 6: *A comparison of the scattering angle (xy-projection) through 20 cm (cube) of Pb, for three versions of* GEANT4*.*

4.1 Recommendation

The change to the GEANT4 default settings and included physics processes have not caused a significant change to the muon multiple scattering results. Any differences that we have observed have been significantly smaller than our detector's angular resolution, and therefore can be neglected.

5 Monte Carlo Physics Lists

The GEANT4 software package requires that the user define the physics processes that he/she would like to include in the simulation. We set our simulation to include all electromagnetic (EM) processes, as those are the main ways in which muon deposit energy. We should note that we do not include any neutron physics, as we have assumed that neutrons cannot interact in a way that would pass the CRIPT DAQ trigger. Including neutron physics can cause a significant loss performance, as neutrons have long mean free paths.

The only remaining question that we had was if we needed to include muon-nuclear interactions. To test this we used the same set-up as in Section 4, and turned the muon-nuclear physics on/off in GEANT4.10.00. The scattering angle was measured with respect to the primary generate muons (0,-1,0). and the direction cosine was determined. The result is presented in Figure 7.

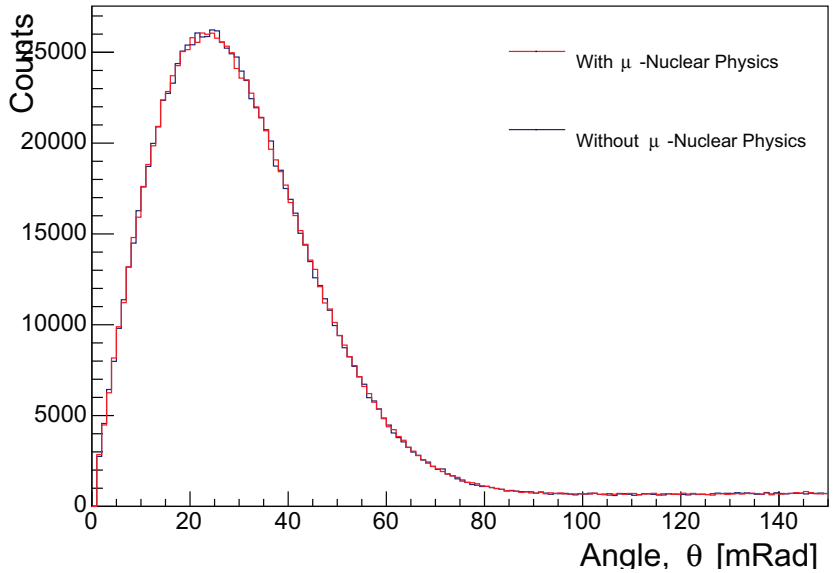

Figure 7: *A comparison of the scattering angle (direction cosine) through 20 cm (cube) of Pb, using GEANT4.10.00. In one case we include muon-nuclear interactions, in the other case we do not include muon-nuclear interactions.*

From Figure 7 we can see no significant difference between including or omitting the muon-nuclear physics.

5.1 Recommendation

As Figure 7 show no significant difference, we choose to include the muon-nuclear term, as it does not affect the run performance. It may be worth time looking at the inclusion of

neutron physics, if the CRIPT collaboration is interested in looking at neutron producing cargo or the CRIPT trigger conditions set to be more inclusive (higher acceptance).

6 Monte Carlo vs. Data

The goal of any physics Monte Carlo simulation is to accurately reproduce the physics in the provided geometry. In the case of CRIPT, we have taken a lot of data and have many figure-of-merit distributions that we can produce in both the data and MC. The following sub-sections describe these figure-of-merit distributions, show some preliminary results for the intrinsic resolution, and finally present a comparison of data and MC for materials that have been imaged in the cargo bay. Sections 6.5 and 6.6 provide details on how the images were made and how we can use the images to identify the material in the image, respectively.

6.1 Charge Collection and Distribution

When a muon interacts with the plastic scintillator bar it deposits some of its energy into the plastic ($\frac{\mathrm{d}E}{\mathrm{d}x}$). This energy is converted to light, which can travel and scatter within the plastic and enter a fibre optic cable that guides the photons to a PMT that coverts this light to a charge. This charge is then proportional to the energy deposited by the muon. The amount of charge collected per unit energy deposited varies from bar-to-bar due to collection efficiencies in the bar and PMT, as well as light loss in the bar and the fibre optic cable (attenuation). These bar-to-bar variations can be calibrated out so that we see the same charge per unit energy in all bars.

The mean charge in a given bar, after calibration, should then be the same for each bar on a given panel. This can be seen for the data in Figure 8. The MC directly measures this energy deposited and a separate simulation in anaTriangle considers all the *imperfections* in the light collection and propagation, and electronic effects in the data. These are also calibrated, and these results are shown in Figure 9. We obtain a good agreement between data and MC for the mean charge distributions.

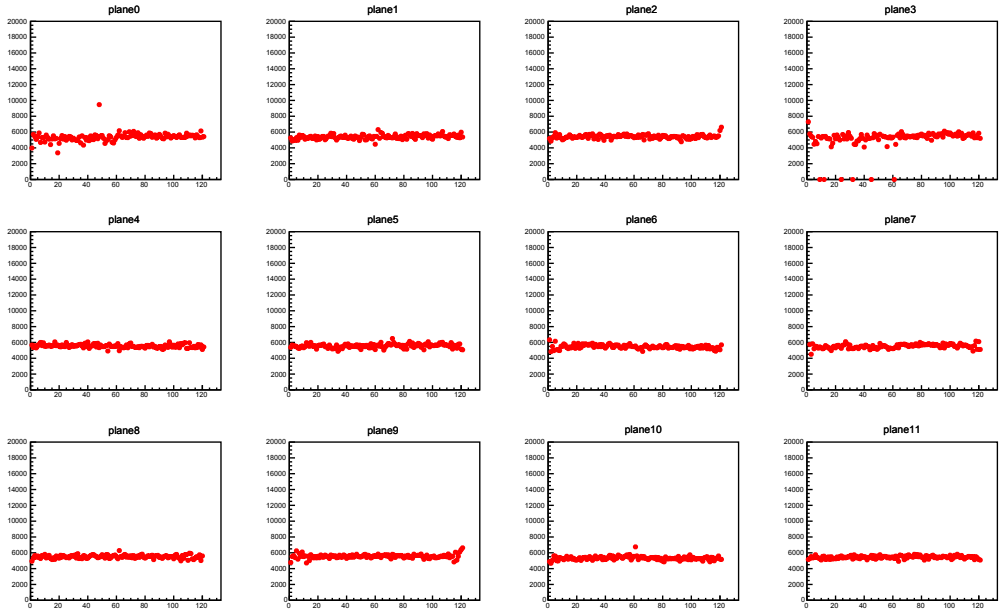

Figure 8: *Charge distribution in the data for a run with an empty cargo bay.*

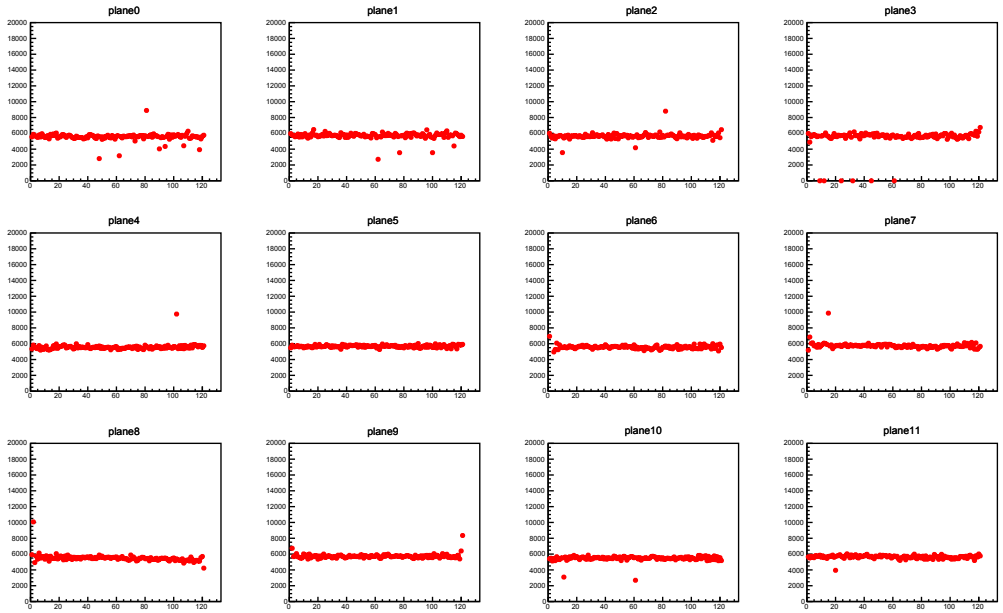

Figure 9: *Charge distribution in the MC for a run with an empty cargo bay.*

6.2 Ratio of Isolated Vs. Adjacent Bars

When a muon passes through a detector panel it can interact with one or two (rarely more) triangular scintillator bars. This ratio is effectively the cross-section of a given bar(s). The cross-section of a single bar can be increase by *enlarging* the apex of the triangle by adding more TiO_2 (shown in Section 3.3) – The TiO_2 does not produce photons when a muon interacts within it. The thickness of this TiO_2 can be measured from samples of the bars, and tuned within the measurement uncertainty.

The ratio of isolated to adjacent bar triggers in the data is shown in Figure 10. If we assume in the MC a thin layer of TiO_2, the same as on the flat sides of the bar, we get ratio much larger than the data, as shown in Figure 11. However, if we then use the measured TiO_2 thickness in the MC we get a much closer ratio, as we can see in Figure 12.

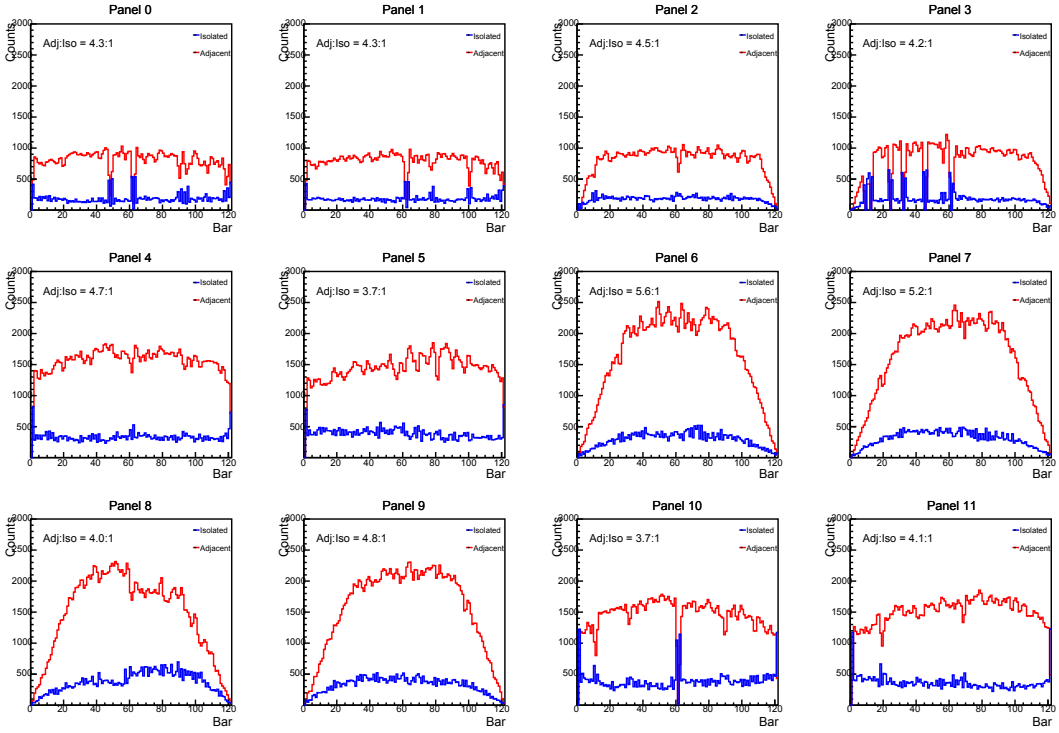

Figure 10: *Using the data, this is the number of counts per bar when either only one bar is triggered (isolated) or two neighbouring bars are triggered (adjacent) for each plane.*

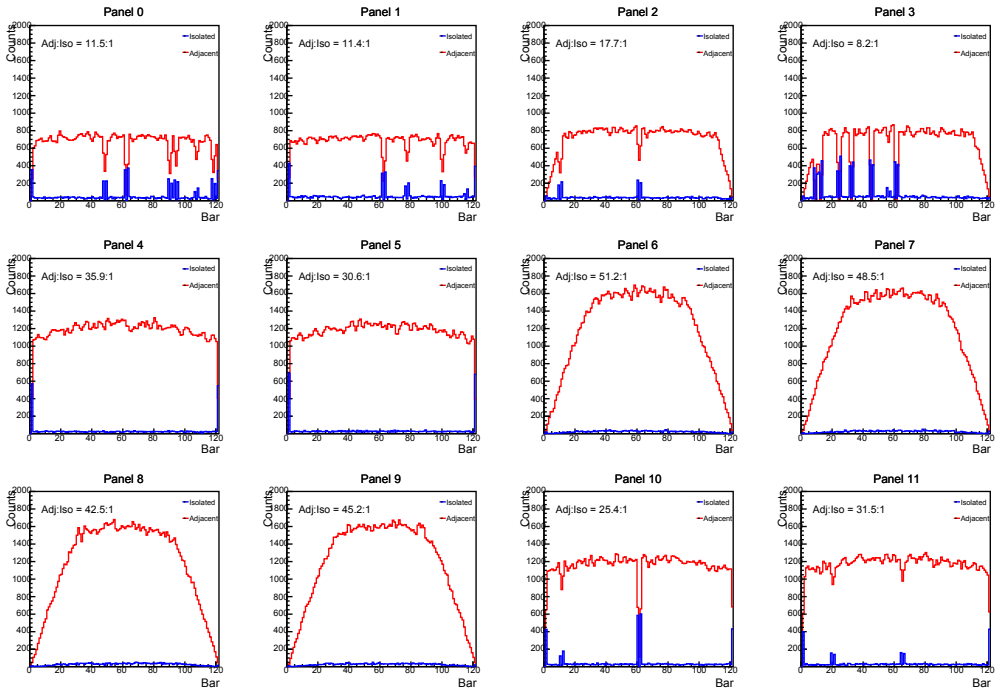

Figure 11: *Using the MC before accounting for extra TiO_2 in the corners of the bar, this is the number of counts per bar when either only one bar is triggered (isolated) or two neighbouring bars are triggered (adjacent) for each plane.*

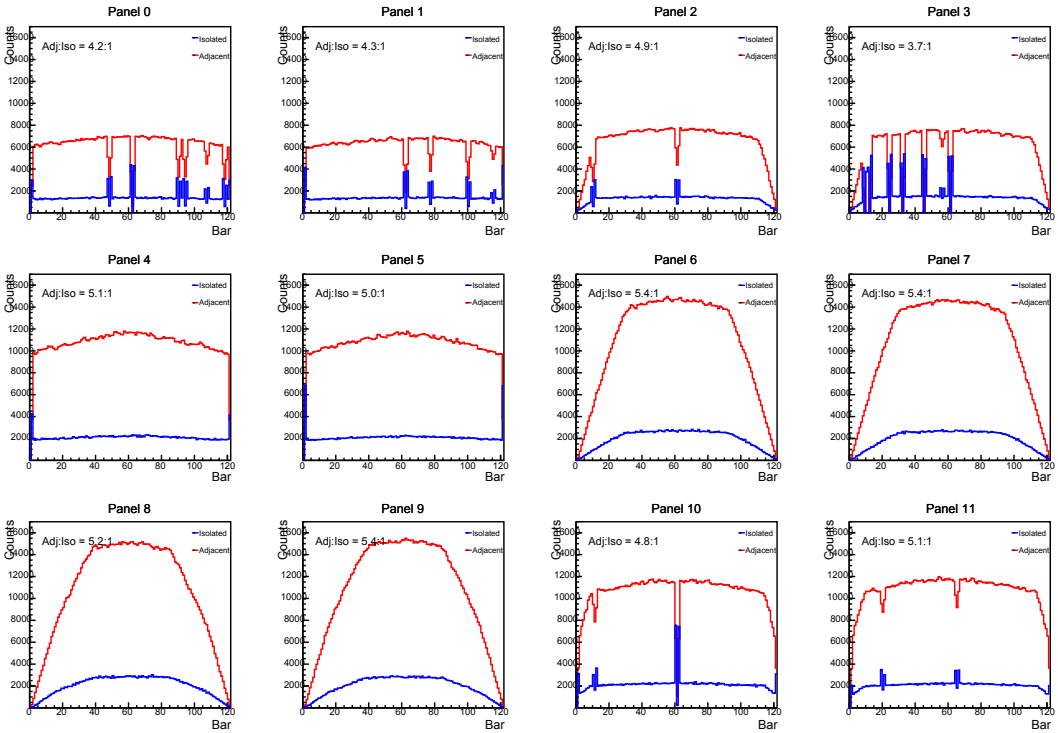

Figure 12: *Using the MC after accounting for extra TiO_2 in the corners of the bar, this is the number of counts per bar when either only one bar is triggered (isolated) or two neighbouring bars are triggered (adjacent) for each plane.*

6.3 Resolution

The intrinsic resolution is the resolution of the detector when you remove the effect of multiple scattering. We believe the MC accounts for the multiple scattering properly, based on the excellent agreement between MC and data in all the figure of merits that tested. This means that we define the intrinsic resolution, R_{in}, by Equation 1:

$$R_{\text{in}} = x_{\text{true}} - x_{\text{pos}} \tag{1}$$

where x_{true} is the true location of the interaction and x_{pos} is the detected location of the interaction. In the case of a single bar, this is just the position of that bar. If multiple bars are triggered then the position is charged weighted between the two bars. We define the true position, x_{true}, by drawing a line between the first scatter in the panel and the last scatter. We then determine the coordinate at mid-point of the plane (there are 12 planes in CRIPT), and call this the true location.

Figure 13 (top) shows the results for Equation 1, for the case of isolated bars per trigger and adjacent bars. We can see that we get better resolution when we use events that hit more than one bar, this makes sense as we can get better position information. Figure 13 (Bottom) shows the same information for resolution, but includes the location along the length of the panel. The values in Figure 13 (Bottom) are the mean $\pm$ RMS of the distributions.

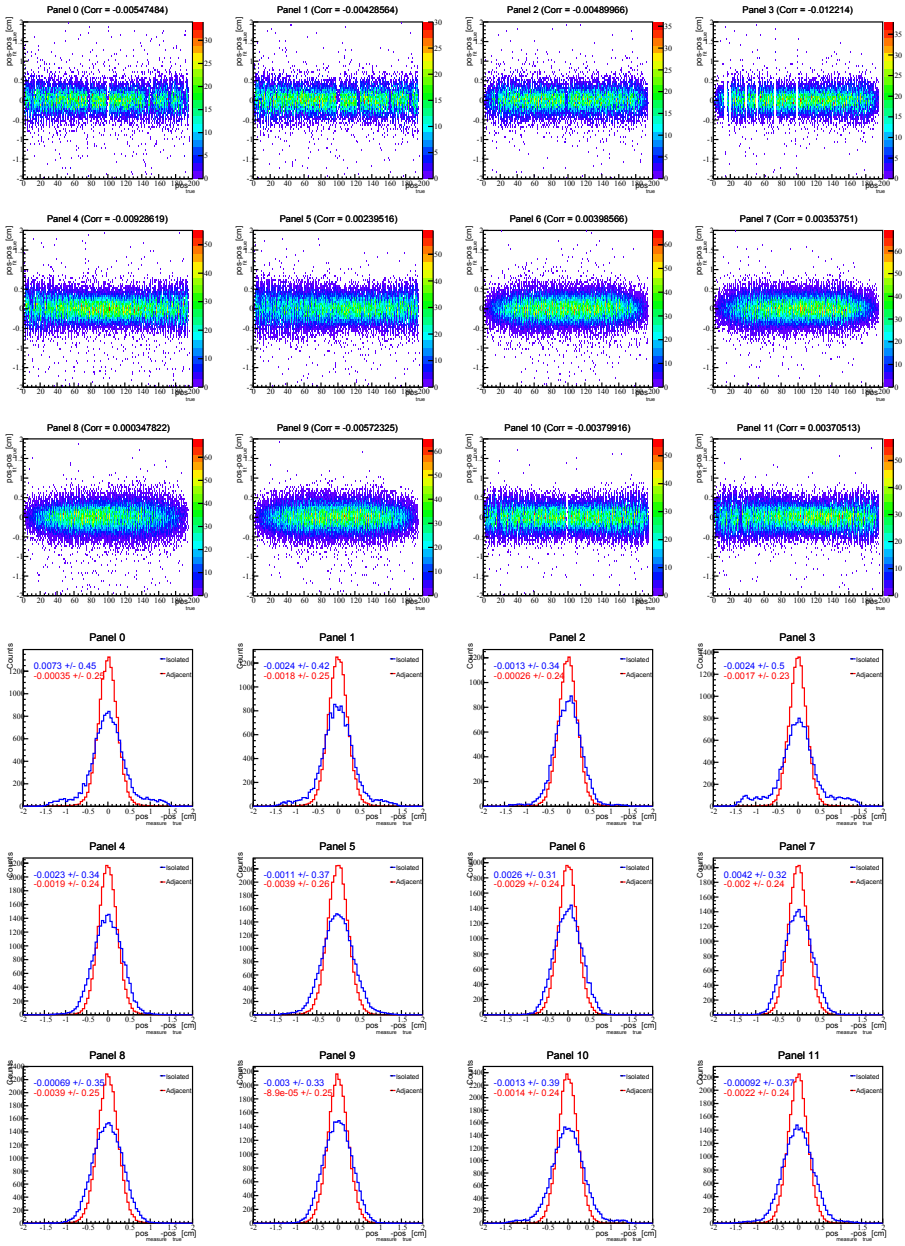

Figure 13: *Top: MC resolution along the length of the bar for each panel. Bottom: Projection (y) of the top figure, divided between isolated bars and adjacent bars.*

6.4 Cargo

The CRIPT detector is designed to image material that is located in it's cargo bay. That is, the space located between the UT and LT. Various items have been imaged, and a selection of these have been added to the MC. One item is a depleted uranium (DU) sphere, with a hole part way through the sphere. This hole is used to test the resolution of the imaging algorithms. The remaining items that have been included in the MC are $10 \times 10 \times 10$ cm cubes of W, Al, Cu, Fe, Pb, or brass. There were multiple runs were different combinations of these cubes were included (sets of three or four). To further test the sensitivity of our imaging algorithms various arrangements of lead bricks were used. Such as, arranging the bricks at varying distances from each other to test if the resolution is good enough to distinguish the individual bricks and bricks making up larger cubes, some with bricks removed to test the imaging resolution. A 55 Gal. drum was filled with wax and had a W rod placed within the wax. This would test if we can see a heavy material embedded in a matrix. The bricks were also arranged to spell CRIPT, this is ideal for testing for rotations between the data and the MC through the imaging routines – it also is nice for presentations.

Table 1 lists the run numbers and cargo type for selected runs. The comparison of the data and MC for each of the runs are shown in Figures 14 to 20. The XY-plane is the horizontal plane, and the Z-axis is the projection of the median scattering angle from voxels onto the 2D XY-plane (pixels).

Run Numbers	Cargo	Data Triggers	MC Triggers
271	Pb (spelling CRIPT)	2,164,543	2,350,364
277	W, Cu, Al, brass	2,035,677	2,848,998
302	W, Cu, Fe, Pb	8,551,823	8,403,324
342	Phantoms (Pb bricks placed various distances apart)	4,339,961	5,684,579
366	Two 20×20 cm lead cubes, one is hollow	12,218,289	11,374,846
482	55 Gal. Drum with wax and W rod	11,446,474	10,346,546
486	DU sphere (horizontal cutout)	16,151,410	760,540
N/A	Fuel Bundle (36 steel rods)	N/A	6,659,747

Table 1: *Run numbers, cargo, and number of data and MC triggers used for images.*

In Figure 14 we see that we get a very close reproduction of the Pb CRIPT letters, although the spacing seems a little different in the MC vs. the data. This is due to the placement of the Pb bricks in the MC, not an imaging artifact.

Figure 15 shows the arrangement for run 277. We can see that for the same number of triggers in the MC and data the images look very similar. A distinct feature in this arrangement is that CRIPT does not have much sensitivity to Al, which is evident in both the data and the MC.

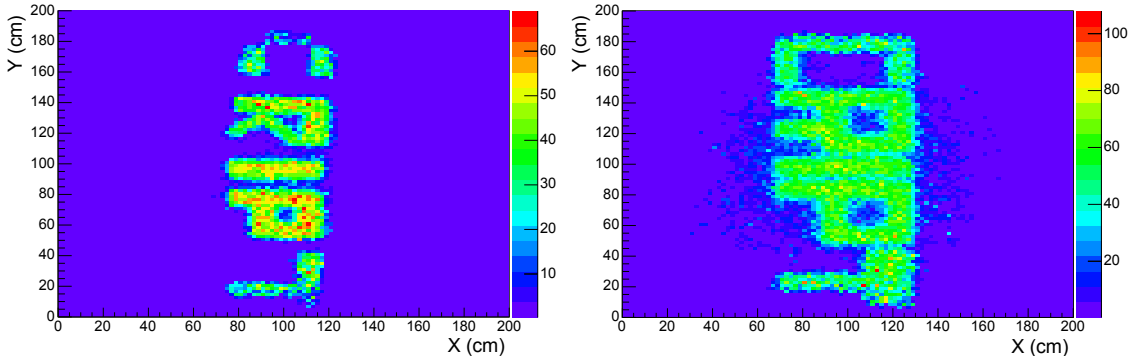

Figure 14: *Imaging run 271. Data on the left, MC on the right. XY are the horizontal planes in this image, Z is proportional to the scattering angle. Pb bricks spelling CRIPT. The spacing between letters looks different between data and MC.*

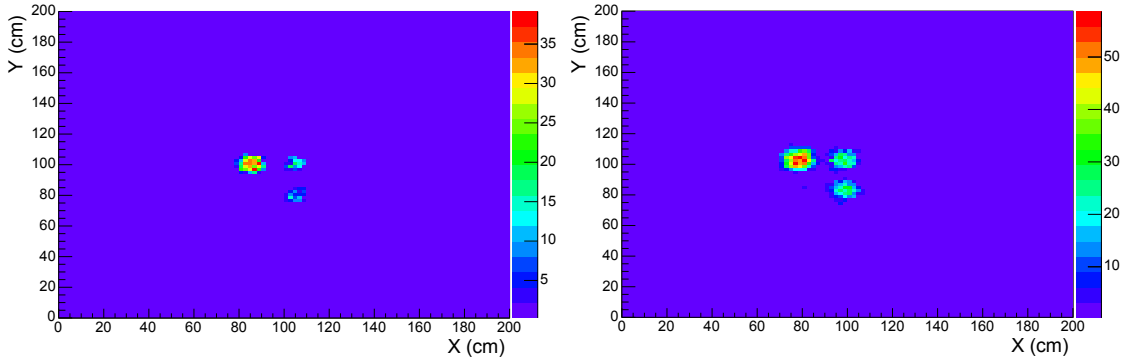

Figure 15: *Imaging run 277. Data on the left, MC on the right. XY are the horizontal planes in this image, Z is proportional to the scattering angle. From top left to bottom right: W, Cu, Al, and brass.*

The images in Figure 16 show the arrangement for run 302 with similar results to Figure 15, that is, that the imaging routine give consistent results between data and MC.

For run 342 we used Pb bricks with various spacing, the results are shown in Figure 17. The goal is to determine the ability of CRIPT to separate individual Pb bricks. The spacing between the bricks ranges from 1–12 cm. In both the MC and the data, the smallest spacing distinguishable is 6 cm. This agreement between data and MC provides further confidence that the MC reproduces the data well.

In Figure 18, run 366, we test CRIPTs sensitivity to hollow section in a Pb block. Both the data and MC are able to observe this hollow space in their images. Like Figure 17, this provides a strong statement that the MC agrees with the data.

Figure 19, run 482, shows the image of a 55 Gal. drum with a $1 \times 1 \times 8$-inch W rod near

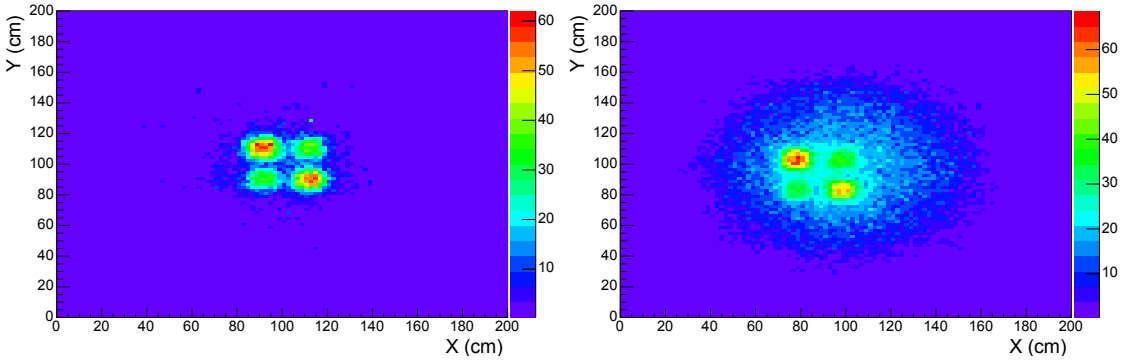

Figure 16: *Imaging run 302. Data on the left, MC on the right. XY are the horizontal planes in this image, Z is proportional to the scattering angle. From top left to bottom right: W, Cu, Fe, and Pb.*

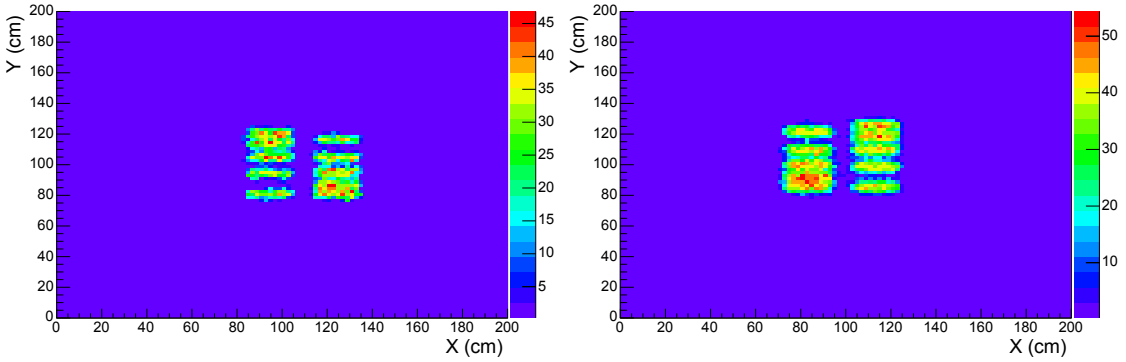

Figure 17: *Imaging run 342. Data on the left, MC on the right. XY are the horizontal planes in this image, Z is proportional to the scattering angle. Pb bricks placed various distances apart – which gaps we are able to distinguish is a measure of resolution/precision. There is an x-flip between MC and data.*

the centre of the drum. In the data (left) we can start to see the W rod, however in the MC (right) it is hard to locate the rod. This is probably due to the distribution of the wax in the data. The wax is made up of many square/cylinder wax blocks, resulting in only 60-70% of the volume being filled. The MC fills the volume completely with paraffin wax. This difference doesn't seem to matter in the imaging, which makes sense, as we saw about our imaging is not sensitive enough to see Al, so wax should not influence the image.

Finally, Figure 20 looks at a depleted uranium (DU) sphere, with a hole bored into one side. Both the data and the MC have trouble imagine the hole. Even though this may seem disappointing, the goal of this study is to produce a MC that matches well to the data, so matching it's limitations evidence of a successful MC.

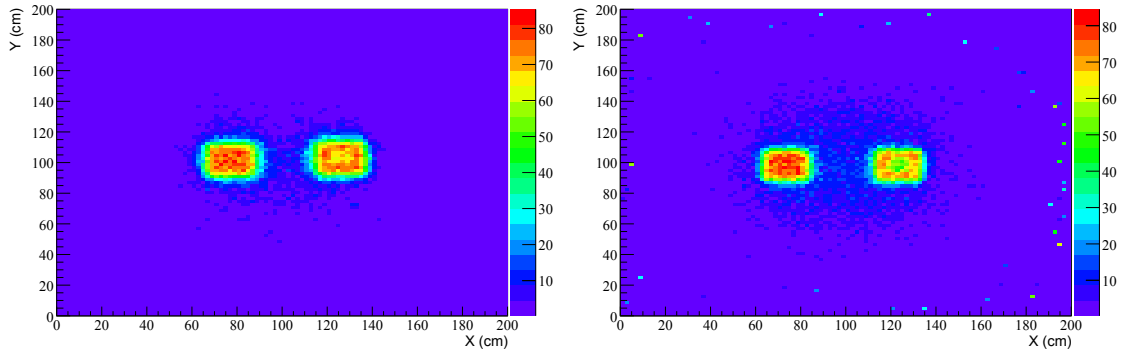

Figure 18: *Imaging run 366. Data on the left, MC on the right. XY are the horizontal planes in this image, Z is proportional to the scattering angle. Two* $20 \times 20 \times 20$ *cm lead cubes, one is hollow (x*$\approx$ *80 cm), the second is solid (x*$\approx$ *120 cm). Right hollow, left solid.*

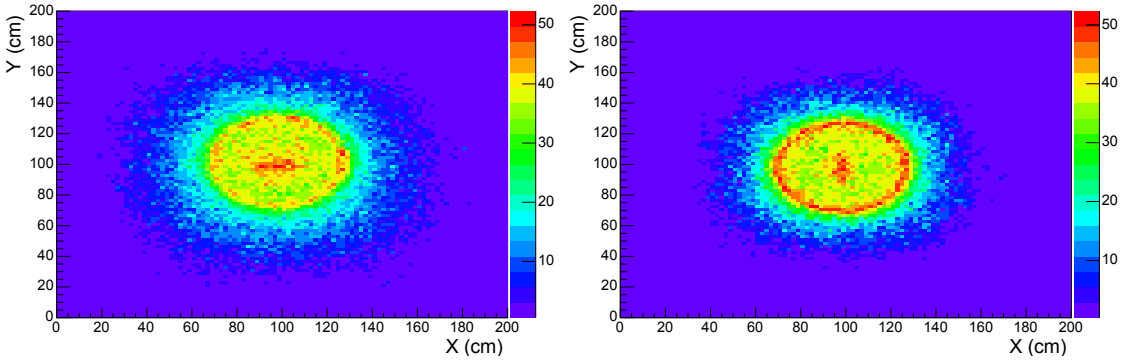

Figure 19: *Imaging run 482. Data on the left, MC on the right. XY are the horizontal planes in this image, Z is proportional to the scattering angle. 55 Gal. drum filled with wax, with a* $1 \times 1 \times 8$*-inch W rod near the centre of the drum.*

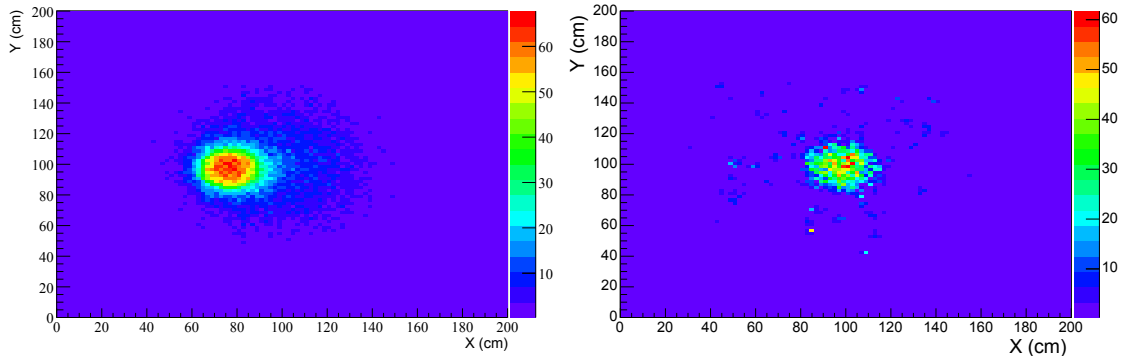

Figure 20: *Imaging run 486. Data on the left, MC on the right. XY are the horizontal planes in this image, Z is proportional to the scattering angle. Depleted uranium (DU) sphere, with cutout in the horizontal direction (parallel to XY-plane).*

6.4.1 Future Runs

Now that the CRIPT detector is located at AECL's Chalk River Laboratories, it is now possible to image CANDU reactor fuel bundles. An example bundle created with (solid) steel rods in the same geometry as the (hollow) fuel rods is available. Figure 21 shows the fuel bundle geometry in the MC. Figure 22 show the image of the steel fuel bundle for a 24 hour run, with the bundle in the vertical position.

After 24 hours and zooming in on the image, it is still not possible to distinguish the individual fuel rods. Longer runs are currently underway at Chalk River.

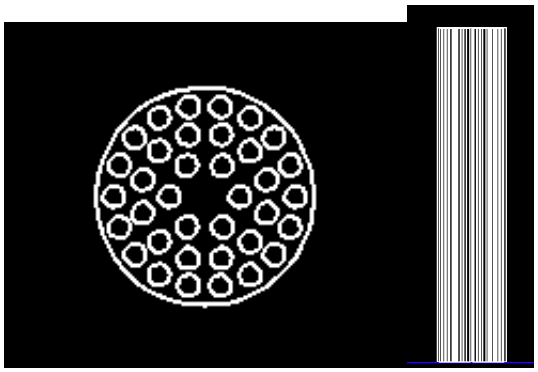

Figure 21: *Fuel bundle geometry in the MC. Top view on the left, and side view on the right.*

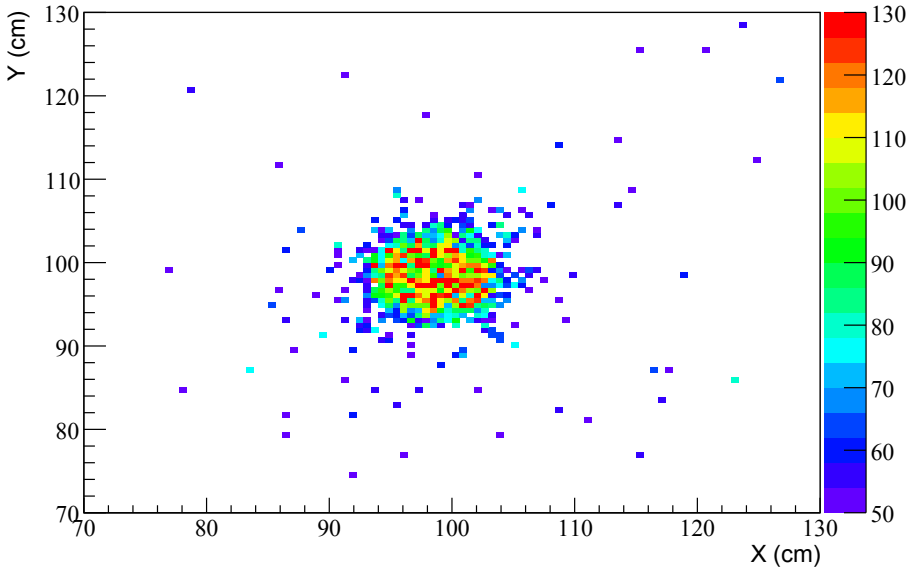

Figure 22: *Imaging of steel MC fuel bundle. 0.6 cm^3 bins.*

6.5 Imaging Using Median vs. Mean Scattering Angle

When creating the 2D images in Section 6.4 we first start with a 3D version. To create an image we use the results from a fit algorithm known as PoCA, a simplified description of how it works is:

1. Assume a linear track from from the upper tracker
2. Assume a linear track from the lower tracker
3. Extrapolate the two lines from 1. and 2. into the cargo area, until they meet.
4. The angle between the lines from 1. and 2. is the called the scattering angle.
5. The value of this scattering angle is recorded in the voxel at the intersection point in the cargo bay

Once all of the triggered muons have been processed each voxel can contain a number of entries (scattering angles). Some examples of these are shown in Figure 23. Each voxel is then represented by a single number to represent the distribution. There are two obvious choices: the mean and the median. The mean can be skewed by tails in the distribution, however the median is always located with 50% above and below, so we like to use the median, as it is more robust. Figure 23 shows two lines, the mean and the median, to illustrate this point.

To create the 2D images, we then project (sum all bins along Z) the 3D voxels onto the XY plane. Cuts can be made to clean up the image to reduce noise. The most effective cut we have found is to check that neighbouring voxels have count rates above a predefined threshold, this eliminates isolated voxels with a high rate, a common noise characteristic. However, how to apply this cut can be tricky.

There are two way to accomplish this cut, first by summing all the scattering angles (SA) in a voxel and comparing it (and its neighbours) to a threshold, as:

$$C = \sum_i \mathrm{SA}_i, \tag{2}$$

and second, by calculating the median (or mean) of each voxel, then comparing that to a threshold:

$$D = \sum_i \frac{\mathrm{SA}_i}{N_i}. \tag{3}$$

It turns out that applying cuts from Equations 2 and 3 do not give the same result. This is because D has added *a function of the number of counts* in the voxel, which varies from voxel-to-voxel and thus creates a varying threshold. This creates more noise in the image,

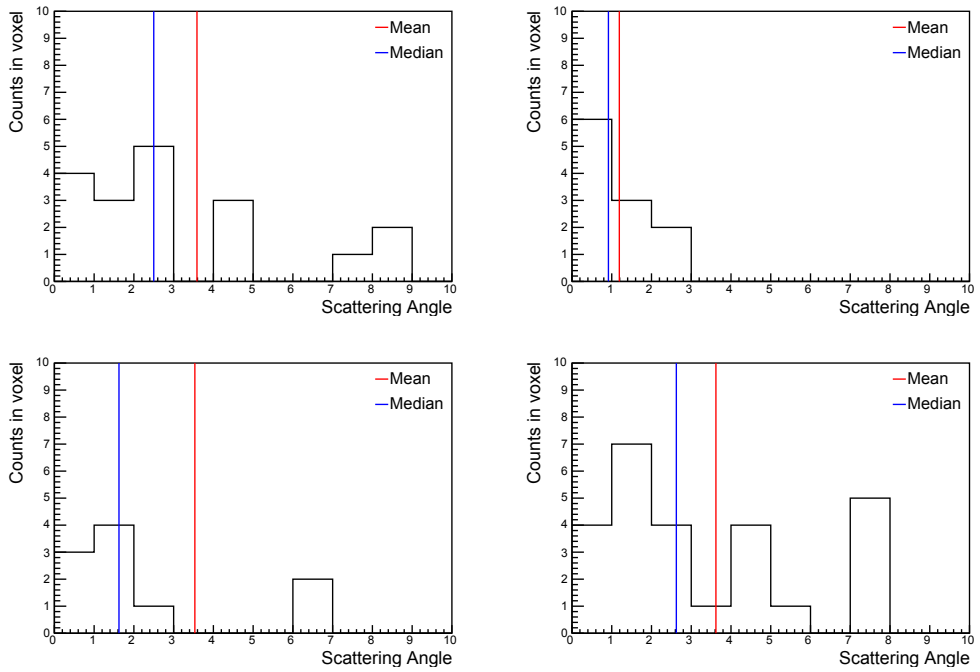

Figure 23: *Distribution of scattering angles for selected voxels.*

often presented as a *halo* in the image. We apply cut C in our algorithm, and then calculate the median in each voxel. We then project this result to create the 2D image.

If we apply the same cut (C) and compare the image using the mean or median, so that the only difference comes from this effect, we get the images in Figure 24. By eye, it looks like the figure on the right (median) has a better signal-to-noise ratio then the figure on the left (mean). To confirm this a ROC curve would have to be created.

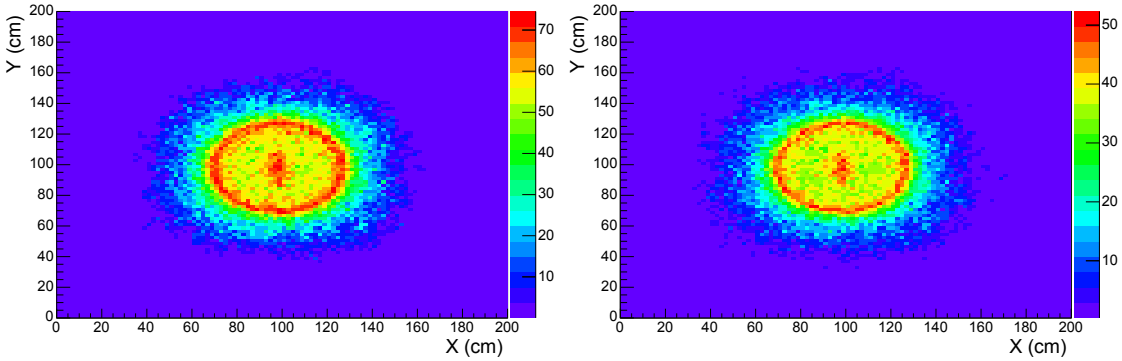

Figure 24: *Mean vs. Median image for run 482. Mean on the left, Median on the right. XY are the horizontal planes in this image.*

6.6 Material (Cargo) Identification

Using the cargo from Section 6.4, it is possible to investigate the scattering angle distributions of various materials. Figure 25 shows the distributions for the objects in run 277 (Figure 15; from top left to bottom right: W, Cu, Al, and brass). This figure is made by looking a region around each cube in Figure 15, and uses the same number of events in both the data and MC. *I.E.* The image of the MC in Figure 15 was recalculated using only the first 2,035,677 events to match the data. The value of each pixel (2D bin) in Figure 15 is the scattering angle. Each of these pixel values in the region containing the respective cube is placed in the corresponding histogram in Figure 25.

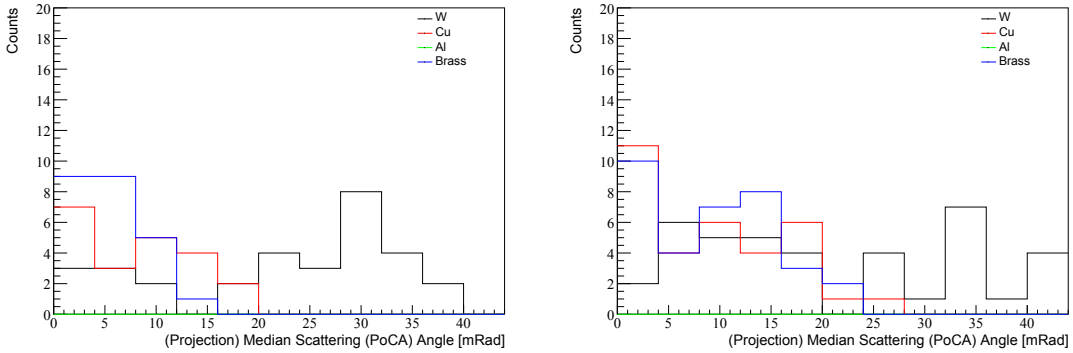

Figure 25: *Distribution of median scattering angles for objects in Figure 15. Data on the left, MC on the right. XY are the horizontal planes in this image.*

Figure 25 shows two sets of distributions: data on the left and MC on the right. Both show the same trend, the heavier materials have larger scattering angles, as we expect. Note that the *Counts* on the y-axis come from the number of bins in the 2D image. To determine an uncertainty we would have to determine the uncertainty in the scattering angle distribution (such as the ones shown in Figure 23).

6.7 Summary

Sections 6.1 and 6.2 provide us with characteristic distributions to aid in MC tuning. Tuning the MC is a necessary process to make the MC replicate the data. The tuning provides a way for the MC to account for parameters that are not simulated, such as photon attenuation lengths and DAQ limitations, among others. The tuning should not account for inaccuracies in the MC geometry, the geometry needs to be as correct as possible to allow tuning to obtain the greatest accuracy and precision. The tuning is carried-out during *post-processing* using anaTriangle.

Using the imaging algorithm on the MC gives similar results to the images of the data. We can see from Figures 14 to 20 that we get a good qualitative agreement. Further studies will be necessary to quantify this agreement.

Section 6.6 provided us with a first look at how CRIPT can be used to identify materials in the cargo bay. This is promising, as this is the goal of CRIPT. It is also encouraging that the distributions make physical sense, that is the heavier materials to correlate to larger scattering angles.

7 Material Scattering and Detection due to Muon Momentum

Section 6 presented the data vs. MC results, and how we can use CRIPT to identify materials in the cargo bay. Here, I studied run 277, building on Section 6.6, we can examine how the muon momentum affects the scattering in the cargo material. Figure 26 shows the muon momentum distribution for events that cause a trigger in CRIPT.

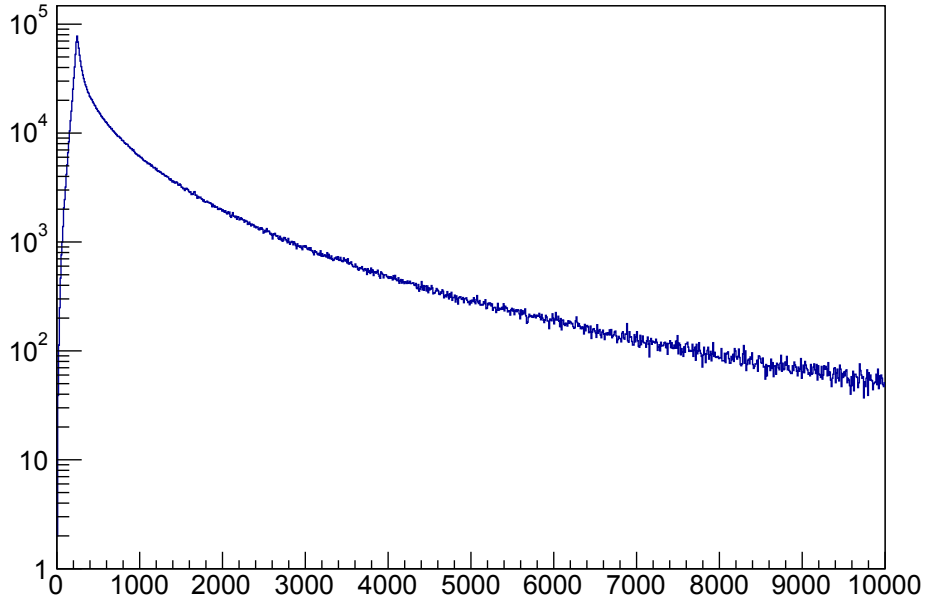

Figure 26: *Distribution of triggered muons for run 277.*

Figures 15 and 25 show the 2D image reconstruction and material scattering distribution for run 277. The following figures will show subsections of these, cutting on the generated momentum of the muon, p_μ. I should note here, that this can only be done for the MC, as it allows us to know the exact generated muon momentum. Figure 27 shows the generated muon momentum for the range $0< p_\mu <500$ MeV, Figure 28 shows the generated muon momentum for the range $500< p_\mu <1000$ MeV, Figure 29 shows the generated muon momentum for the range $1000< p_\mu <2000$ MeV, Figure 30 shows the generated muon momentum for the range $2000< p_\mu <3000$ MeV.

We can see that for 500 MeV$< p_\mu$ that we get no information. This is mostly likely due to an excess of scattering and absorption of muons that interact in the material, due to the low energy of the muon. At higher energy, those with $p_\mu >2000$ MeV we see also see obtain no information about the material. This is due to the high energy muons scattering

very little in the material. This study informs us that muons with a incoming momentum of 500< p_μ <2000 MeV are the important events from CRIPT.

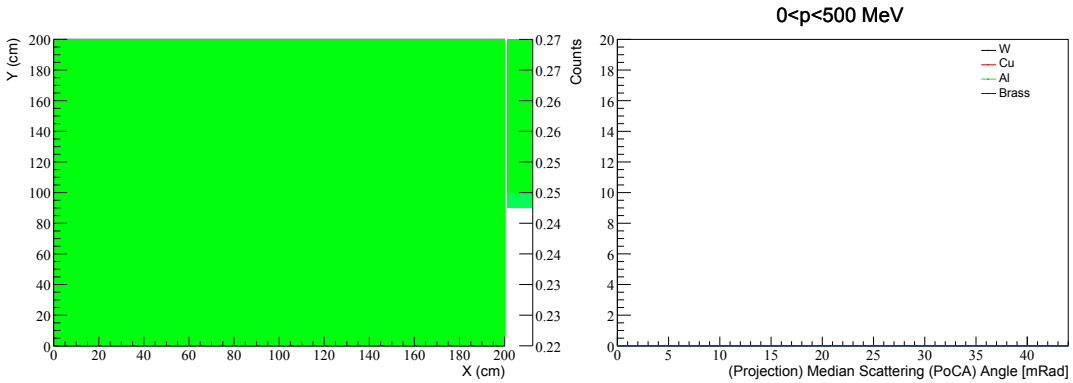

Figure 27: *Distribution of median scattering angles for objects in Run 277 for the momentum range: 0< p_μ <500 MeV. Image on the left, median scattering angle on the right. XY are the horizontal planes in this image.*

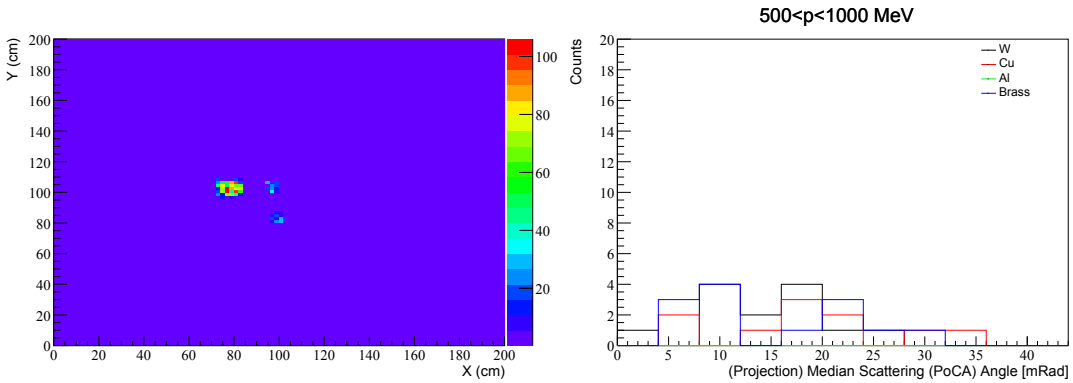

Figure 28: *Distribution of median scattering angles for objects in Run 277 for the momentum range: 500< p_μ <1000 MeV. Image on the left, median scattering angle on the right. XY are the horizontal planes in this image.*

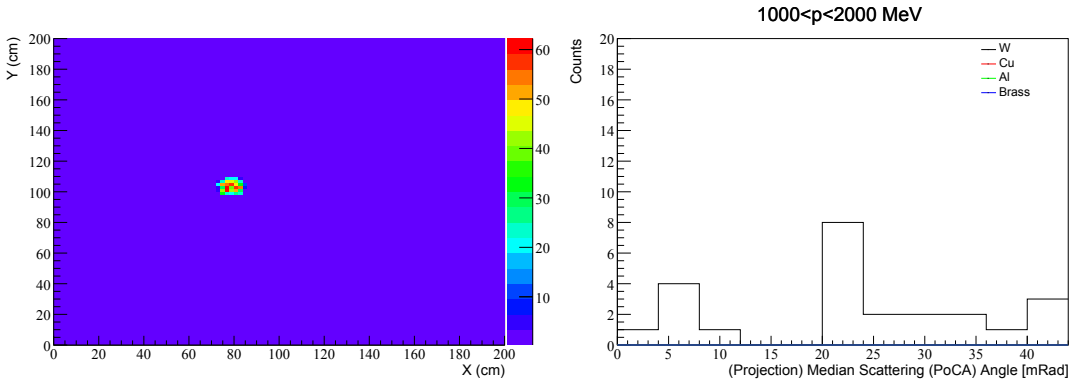

Figure 29: *Distribution of median scattering angles for objects in Run 277 for the momentum range: 1000< p_μ <2000 MeV. Image on the left, median scattering angle on the right. XY are the horizontal planes in this image.*

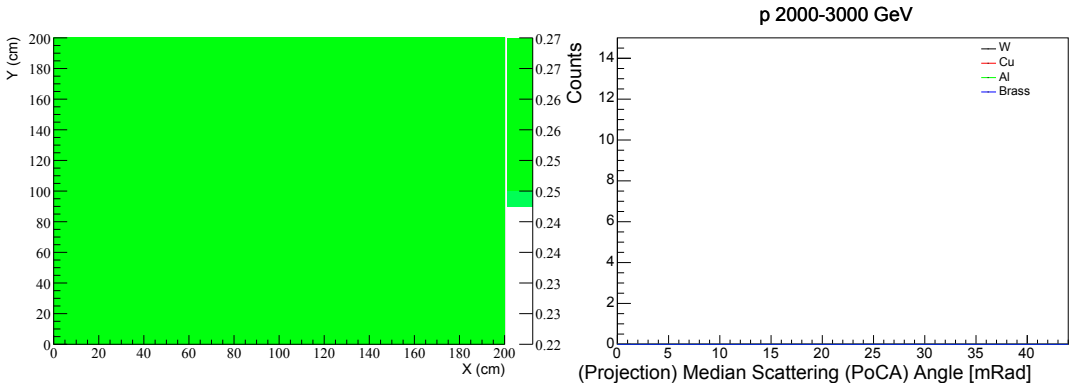

Figure 30: *Distribution of median scattering angles for objects in Run 277 for the momentum range: 2000< p_μ <3000 MeV. Image on the left, median scattering angle on the right. XY are the horizontal planes in this image.*

8 Conclusion

This work has created a Monte Carlo simulation that contains all the relevant physics process necessary for muon scattering, and includes all the detector and structure geometry as provided by the CAD drawing used for construction. The MC can produce output that can be read and processed by the same software tools (anaTriangle) that process the data from the DAQ system.

With proper tuning we achieve excellent agreement between the MC and data for characteristic distributions. This includes the reproduction of the scattering angle of objects placed in the cargo bay. The ability of the MC to reproduce the data allows for further testing our imaging algorithms and sensitivity to various material, such as SNM, without spending the time and money collecting data. The MC is an excellent tool to use to determine which samples we should examine, and it aids scheduling and run planing.

The MC can also be used for planning future experiments, such as expanding CRIPT to include *side detectors* to accept more horizontal muons and obtain larger sensitivity for 3D images. It can also be used to calculate the sensitivity of scaled down muon-tomography experiments.

References

[1] Agostinelli, S. et al. (2003), Geant4: a simulation toolkit, *Nuclear Instruments and Methods in Physics Research Section A: Accelerators, Spectrometers, Detectors and Associated Equipment*, 506(3), 250 – 303.

[2] Allison, J. et al. (2006), Geant4 developments and applications, *Nuclear Science, IEEE Transactions on*, 53(1), 270 –278.

[3] D. Bryman, Z. L., J. Bueno (2010), Scintillator detector: Analysis and resolution measurement, Technical Report Advanced Applied Physics Solutions. internal report, unclassified.

[4] Bryman, D. et al. (2011), Data acquisition system for the CRIPT project, Technical Report Advanced Applied Physics Solutions. internal report, unclassified.

[5] Brun, R. and Rademakers, F. (1997), ROOT - An Object Oriented Data Analysis Framework, *Nuclear Instruments and Methods in Physics Research Section A: Accelerators, Spectrometers, Detectors and Associated Equipment*, 389, 81–86.

[6] (1996), ROOT - An Object Oriented Data Analysis Framework, AIHENP'96 Workshop. See also http://root.cern.ch/.

[7] Hydomako, R. (2014), Alignment and momentum estimate evaluation for the CRIPT detector. DRDC Contract Report.

This page intentionally left blank.

Distribution list

Internal distribution

1 David Waller

2 DRDC Library

Total internal copies: 3

External distribution

Department of National Defence

1 DRDKIM

Other Canadian recipients

1 Mr. Andrew Erlandson
Applied Physics Branch
Canadian Nuclear Laboratories
20 Forest Avenue
Deep River, ON K0J 1P0

1 Prof. John Armitage
Department of Physics
Carleton University
1125 Colonel By Drive
Ottawa, ON K1S 5B6

Total external copies: 3

Total copies: 6